

Designing Bio-mimetic Variational Porosity for Tissue Scaffolds

AKM Khoda¹ and Bahattin Koc^{1,2}

¹Department of Industrial Engineering, University at Buffalo, Buffalo, NY
14260, USA

²Faculty of Engineering and Natural Sciences, Sabanci University, Istanbul
34956, Turkey

Abstract

Reconstructing or repairing the damaged or diseased tissues with porous scaffolds to restore the mechanical, biological and chemical functions is one of the major tissue engineering strategies. Development of Solid Free Form (SFF) techniques and improvement in biomaterial properties by synergy have provided the leverage to fabricate controlled and interconnected porous scaffold structures. But homogeneous scaffolds with regular porosity do not provide all the biological and mechanical requirements of an ideal tissue scaffold. Thus achieving controllable, continuous, interconnected gradient porosity with reproducible and fabricatable design is critical for successful regeneration of the replaced tissue. In this research, a novel scaffold modeling approach has been proposed to achieve bio-mimetic tissue scaffolds. Firstly, the optimum filament deposition angle has been determined based on the internal heterogeneous regions and their locations. Then an area-weight based approach has been applied to generate the spatial porosity function to determine the filament deposition location for the desired bio-mimetic porosity. The proposed methodology has been implemented using computer simulation. A micro-nozzle biomaterial deposition system driven by NC motion control has been used to fabricate a sample designed structure.

Keywords

Deposition angle, porosity function, bio-mimetic porosity.

1. Introduction

Stimulating the tissue regeneration via scaffold with interconnected and continuous pore has recently been developed as one of the tissue engineering strategies. Few researches [1, 2] have focused on the internal design architecture of the porous scaffold and they concluded that properly interconnected and continuous pore with their spatial distribution might contribute to perform diverse mechanical, biological and chemical functions of a scaffold. Thus the need for reproducible and fabricatable scaffold design with controllable and functional gradient in porosity is required but is hindered by design and fabrication limitations [3].

Researchers [4] have invested in bio-mimetic scaffold design concept via inverting the morphological structure to achieve the desired and choreographed multi-functionality from a scaffold structure. Bone is a hierarchical material whose mechanical properties can vary considerably within the same specimen and does not depend upon its density alone [5]. Anisotropic mechanical properties of bone caused by the difference in micro structure has been reported in [6]. Both cortical and cancellous bone segment has different structural form with distinct characteristics. Moreover, within cancellous bone there exist a complex relationship [7] between trabecular density and its structural mechanical integrity which makes the bone spatially heterogeneous. Thus achieving a bio-mimetic scaffold design by only mimicking the bone morphology may not capture the regional heterogeneity in bone's spatial extrinsic and intrinsic properties. Moreover such complex design requires significant amount of computational resources and might become infeasible in terms of its fabricatability. On the other hand bone structures adapt its strength via remodeling [8] in response to the anisotropic load distribution along every direction. This physiological multi-axial load transfer through the inhomogeneous cross-section of bone along the length supports its spatial and regional heterogeneous structural properties [9, 10]. But such imminent factors are completely ignored in current design of bio-mimetic scaffolds. Thus designing of bio-mimetic scaffold with homogenization of property and/or material distribution might not be the proper functional representation.

In this work, a novel heterogeneous porous structure modeling has been proposed to achieve the gradient porosity design. First, an optimum filament deposition direction has been determined in slices based on the contour geometry and their changes along the homogeneous deposition path. And then internal regions have been discretized as strips considering their spatial homogeneity factor along the optimum deposition angle. Finally, an area weight based approach has been used to generate the spatial porosity function for each strip that determines the filament deposition location for desired bio-mimetic/heterogeneous porosity. The proposed method generates a heterogeneous structure that captures the functional and regional heterogeneity along the structure and conform the shape of the targeted contours. Also a micro-nozzle biomaterial deposition system driven by NC motion control has been used to fabricate a sample designed structure with proper continuity and connectivity.

The rest of the paper is organized as follows. Section 2 contains the novel variational porous scaffold structure modeling with controllable and variational porosity design. In sub-section 2.1, we discussed the geometric model extraction for the defected bone segment. Sub-section 2.2 describes the slice generation methodology along with the internal feature suitable for SFF technique. Section 2.3 and 2.4 describes the contour discretization and determine the optimum deposition angle considering the heterogeneity of the scaffold. Section 2.5 determines the spatial function for optimum filament path to achieve desired porosity. The proposed design has been implemented and results have been shown in Section 3.

2. Methodology

2.1 3D Model Extraction with Internal Iso-Feature

Firstly, medical image obtained from non-invasive techniques such as Computed Tomography (CT), Magnetic Resonance Imaging (MRI) is used to obtain the geometric and topology information of the defected bone segment. The initial geometric information of the model could be represented as a mesh or Stereolithography (STL) model. The STL files are generated by tessellating the outside surface of the 3D volume with triangles.

As discussed earlier, regional heterogeneity exists in bone and allows bone to perform its multi-objective functionality, i.e. mechanical, biological and chemical functions simultaneously. Such regional heterogeneity in bone could be consolidated into combination of internal homogeneous feature to discretize the 3D bone space. The geometric significance (i.e. location, size, shape) of such internal extrinsic feature or the heterogeneity for the defected bone segment can be obtained by analyzing the MRI or CT image for bone mineral density [11], bone texture analysis via micro-beam X-ray radiation [12] or feature recognition algorithms. These spatially distributed 3D features might represent uniform material concentration individually and their combination could capture the anisotropy in bone structure. The accuracy of such representation for bone anisotropy might be a subject of proper data evaluation methodology and beyond the scope of this paper. Thus the defected bone segment or targeted region could be represented by a set of iso-property regions which may not be axisymmetric or uniform shape as shown in Figure 1. The corresponding property for each iso-region can also be interpreted as uniform material concentration or iso-porosity regions and thus the term iso-porosity and iso-property have been used alternatively in this paper. Moreover, any segment or region contain more than one iso-property region are referred as heterogeneous region in this paper.

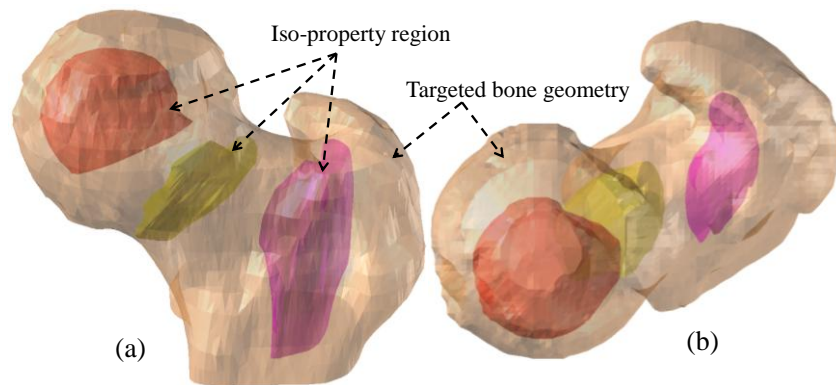


Figure 1: (a) Perspective view (b) top view of targeted bone geometry with internal iso-property region that represent the regional heterogeneity.

2.2 Slice Generation

The generated surfaces along with the internal features are sliced for layer manufacturing by a set of intersection plane perpendicular to the height of the targeted geometry. By connecting the intersection points between the plane and the surfaces would generate non-self intersecting, closed and planar contours. The distance between the intersecting planes can be constant in uniform slicing which is usually the diameter of deposited filament by the SFF system. Thus a set of parallel slicing contours represent the targeted bone geometry $S = \{s_k\}$ where k is the number of contour slice for the bone segment. The k^{th} contour of the bone geometry and the corresponding internal iso-porosity contours have been shown in the following figure (Figure 2) as an example.

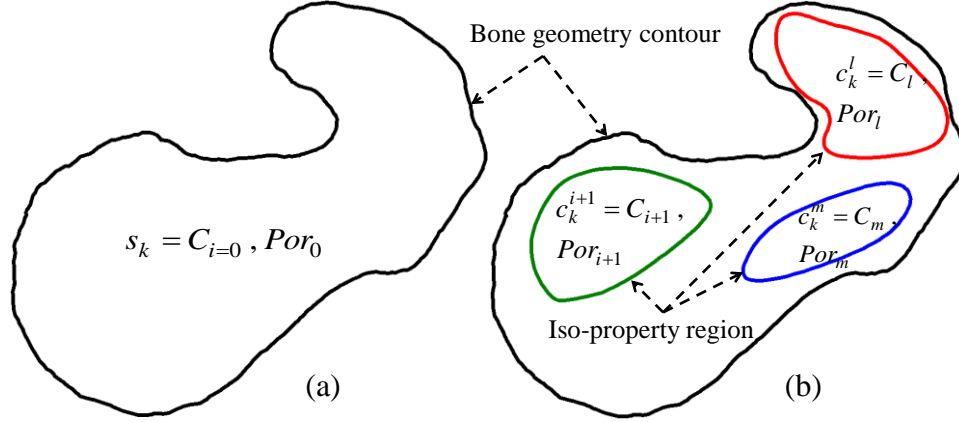


Figure 2: A sample slice of bone (a) only outer contour and (b) the corresponding internal iso-porosity contours.

In such case the outer contour s_k contains the entire iso-porosity contour curves $C_k = \{c_k^1 \dots c_k^m\}$ where m is the number of iso-porosity contours at the k^{th} slice. Thus a set of iso porosity contour curves embedded in the outer slice contour represent each layer with set of contours $C = \{C_0 = s_k, C_k\} = \{C_i\}_{i=0, \dots, m}$ and each contours are assigned with a desired porosity defined by Por_i . All contour curves are simple planner closed curve i.e. they do not intersect itself other than its start and end points and have the same (positive) orientation. The general equation for these contours can be parametrically represented as:

$$\begin{aligned} C_i(u_i) &= (x(u_i), y(u_i)) \quad \forall i = 0, \dots, m \\ u_i &\in [a_i, b_i] \\ C_i(a_i) &= C_i(b_i) \end{aligned} \quad (1)$$

Here, $C_i(u_i)$ represents the parametric equation for i^{th} contour with respect to parameter u_i at a range between $[a_i, b_i]$.

2.3 Optimum Filament Deposition Direction

Currently, designing a homogeneous scaffold assumes the property homogenization that results equidistant filament deposition parameter throughout the internal region. Such property homogenization may address the desired property of a single uniform region, but completely ignores the presence of any regional heterogeneity which could have a cost function that may generate design errors. For multi-regional heterogeneity, these design errors could accumulate and may increase exponentially. To demonstrate, a simple example has been presented in Figure 3, where the outer boundary contour contains four sets of heterogeneous regions. By designing a homogeneous scaffold with equidistant filament location along an arbitrary direction may result in design errors for almost every segment between those filaments as shown in Figure 3(a). Choosing a proper deposition direction or frame angle, this intervening segment area can be reduced significantly which may reduce the error of targeted region shown in Figure 3(b).

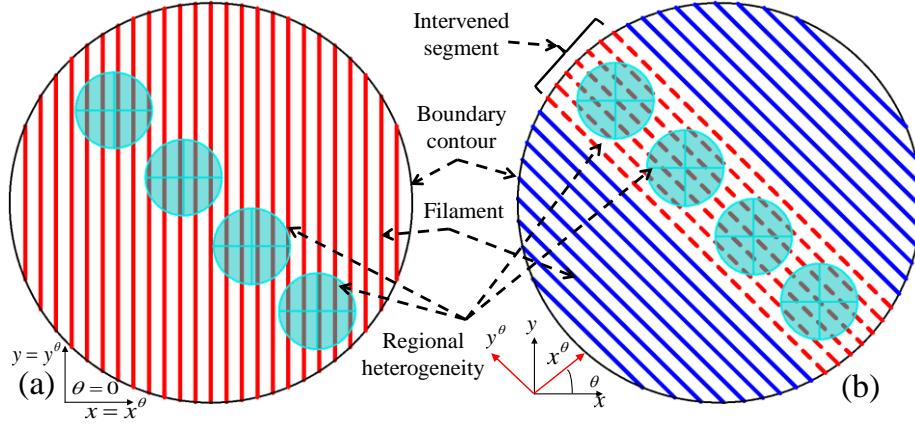


Figure 3: (a) Filament deposition pattern at $\theta=0^\circ$ (b) aligned filament deposition pattern at θ for the same regional heterogeneity in a boundary contour.

Thus to increase the homogeneous deposition path via reducing the heterogeneous region intervention, an optimum filament deposition direction needs to be determined at each layer based on the contour geometry and location of the targeted region.

2.4 Strip Generation and Weight Determination

To determine the cost function based on the heterogeneous region intervention, the targeted region first needs to be discretized based on the heterogeneity factor. The region can be discretized by a set of parallel lines where the area generated between two parallel lines has been denoted as a strip. Then each strip area needs to be analyzed for heterogeneity to determine its cost function. Now these parallel lines might be equidistant from each other or varying distant and could be a design variable. But to avoid virtually infinite combinations a novel technique of ‘strips from contour’s tangent’ [3] approach has been developed. This would eventually reduce the feasible solution space significantly without compromising the optimality as shown in Figure 4.

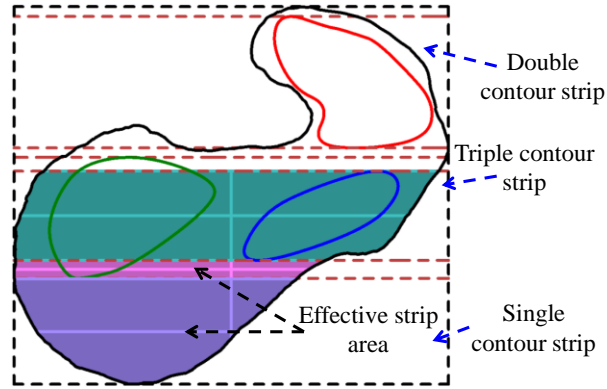


Figure 4: Generating the strips and effective strip area with heterogeneity.

After discretizing the region with strips, the area based heterogeneity weight for each strip has been calculated using the following equation.

$$Weight_ST_j = \left((A_j - \sum_{i=1}^m CA_{A_j}^i) + \sum_{i=1}^m (CA_{A_j}^i \times het_j^{Contour}) \right) \times het_j^{Property} \quad \forall j \quad (2)$$

Where, $Weight_ST_j$ is the weight; A_j is the effective area, $CA_{A_j}^i$ is the area of i^{th} contour contributed to the effective area; $het_j^{Contour}$ and $het_j^{Property}$ are the heterogeneity factor due to contour and property of j^{th} strip. And thus by summing weight for all strips, the total weight of the slice at frame angle θ can be calculated.

$$Total_Weight^\theta = \sum_{j=1}^n Weight_ST_j \forall \theta \quad (3)$$

Here, $Total_Weight^\theta$ is the accumulated total weight evaluated at frame angle θ . This accumulated weight is a non-linear function of contributed area. In ideal case, a complete homogeneous region would give minimum weight. Increasing the heterogeneity would increase the weight of the slice. By using the same methodology described above, the weight can be determined for every frame angle $\theta \in [0, \pi]$ interval and the optimum deposition direction θ^* can be determined by the function, $\text{Min} \{Total_Weight^\theta\}$.

2.5 Function Based Filament Deposition Location

After getting the optimum filament deposition direction, a function based filament distance determination methodology has been implemented to determine the optimum filament location. The functional area for each contributing contours along the width of the strip have been plotted as shown in Figure 5.

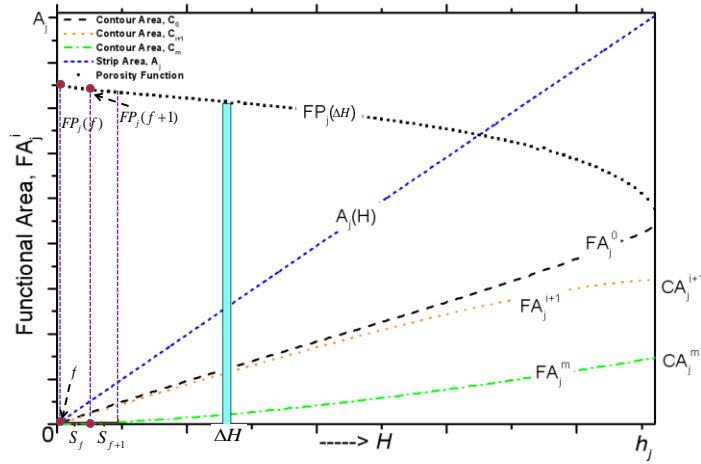


Figure 5: Filament positional function determination for a heterogeneous triple contour strip j^{th} .

The functional porosity, FP for any small segment, ΔH in the strip can be calculated by the following equation where, $\Delta H \rightarrow 0$ and is the function of strip width and its contour property.

$$FP_j(\Delta H) = \sum_{i=0}^m \frac{FA_j^i(\Delta H)}{A_j(\Delta H)} \times Por_i \quad \forall j, FA_j^i > 0; \quad (4)$$

Where, $FA_j^i(\Delta H)$ is the functional area generated by i^{th} contour, $FP_j(\Delta H)$ is the functional porosity for j^{th} strip with equidistant width ΔH and is calculated by considering the weighted area contribution of corresponding contours and porosity. After plotting the porosity function for the strip, the distance between filaments for any spatial segment can be determined by using that function. For evaluation purpose the porosity deviation from the designed one to the desired porosity has been calculated by Equation 5.

$$E = \sum_{j=0}^n \sum_{i=0}^m (|FP_j(f) - Por_i|) \times FA_j^i(f) \quad \forall f \quad (5)$$

Where, E is the resultant porosity evaluation index.

3. Implementation

The proposed techniques have been implemented on a multiple iso-porosity region as shown in the Figure 6 using Rhino3D software and Visual Basic programming language on 2.3 GHz PC. The corresponding property has been presented in Table 1 and the analyses have been performed with Visual-Basic Script to demonstrate the proposed methodology.

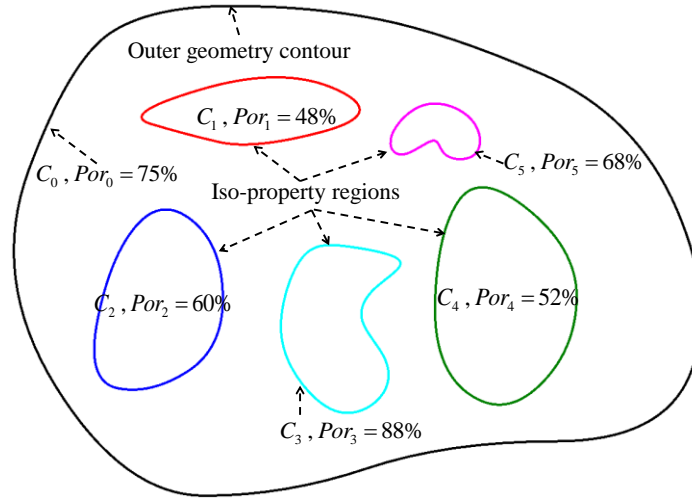


Figure 6: Free-form heterogeneous slice with five iso-porosity region.

Table 1 Corresponding property of the heterogeneous slice presented in Figure 6.

Contour, C_i	Porosity, Por_i	Area, mm^2
C_0	$Por_0 = 75\%$	266.87
C_1	$Por_1 = 48\%$	13.9
C_2	$Por_2 = 60\%$	23.94
C_3	$Por_3 = 88\%$	18.96
C_4	$Por_4 = 52\%$	32.2
C_5	$Por_5 = 68\%$	4.75

The optimum deposition direction or frame angle for a slice k has been determined as $\theta_k^* = 111^\circ$ which has the minimum total weight in Figure 7 and 8.

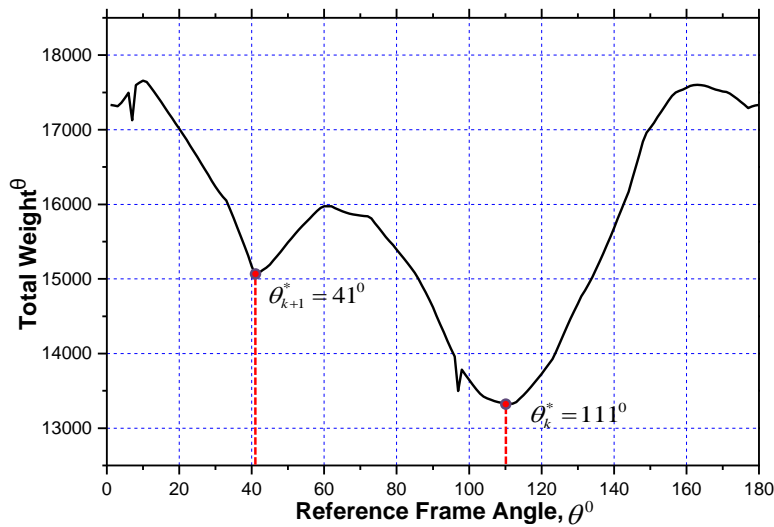


Figure 7: The total weight plot at $\Delta\theta = 1^\circ$.

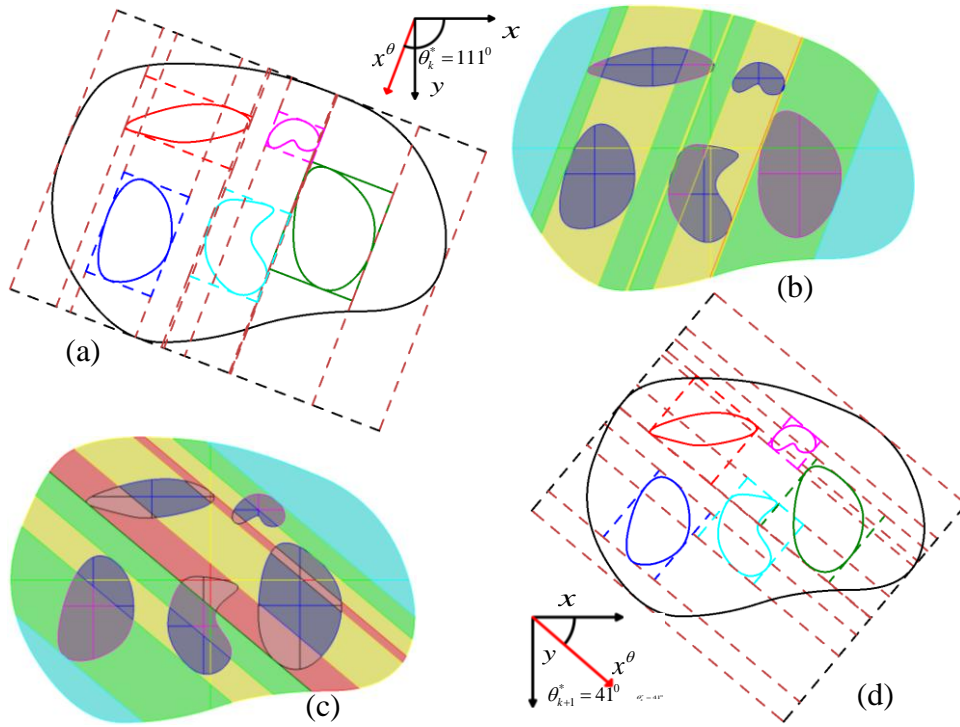


Figure 8: Optimum filament deposition angle (a-b) $\theta_k^* = 111^\circ$ and (c-d) $\theta_{k+1}^* = 41^\circ$ and associated strips respectively.

A total of eleven strips have been generated in the consecutive optimum layer with both homogeneous and heterogeneous strip property. Also individual weight contribution is measured by Equation 2 and shown in Figure 9 for this example.

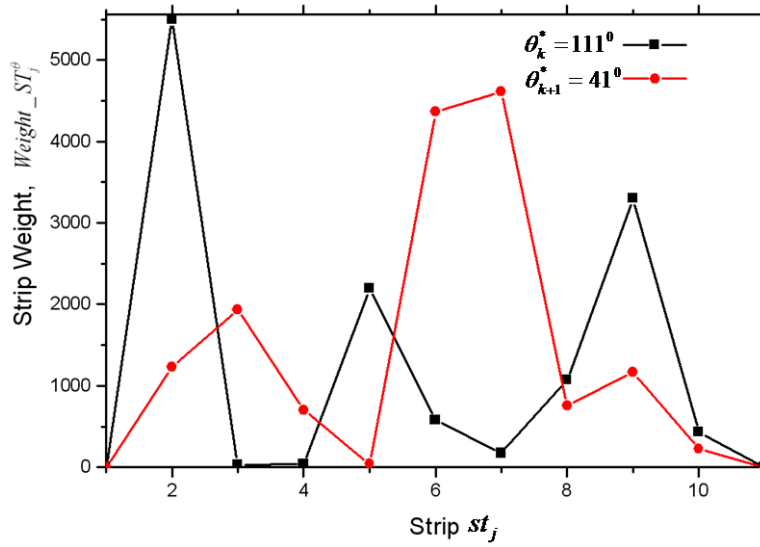


Figure 9: Individual strip weight contribution for both optimum layers.

Spatial porosity function for both layer have been determined using Equation 4 and plotted Figure 10. The lower horizontal axis represents the strip width for the 1st layer ($\theta_k^* = 111^\circ$) and the upper horizontal axis represents the consecutive second layer $\theta_{k+1}^* = 41^\circ$.

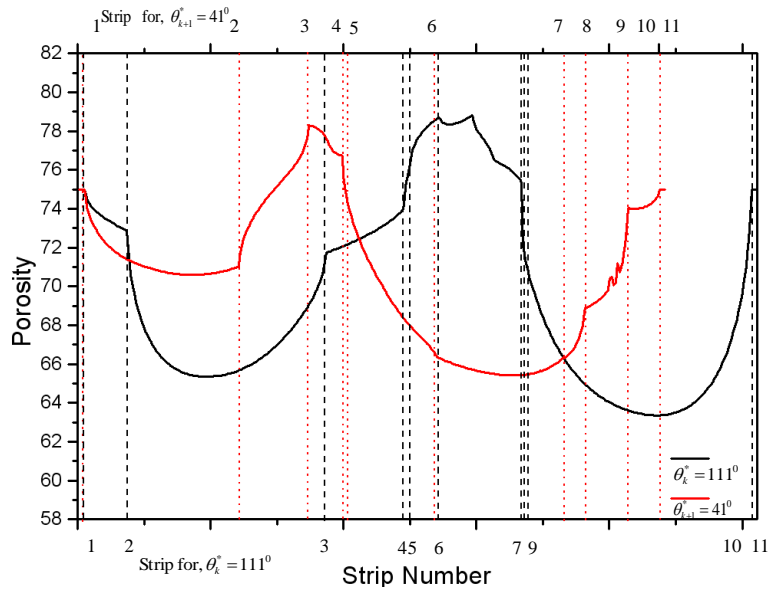


Figure 10: Porosity function for consecutive optimum layer.

By using the porosity function, the filaments location has been determined and drawn as shown in Figure 11. To determine the filament location, the sample has been designed with 100 micrometer filament diameter. Moreover a bi-layer membrane combining the two layers has been shown and the porosity has been evaluated for the generated anisotropic pore-cell as shown in the Figure 11.

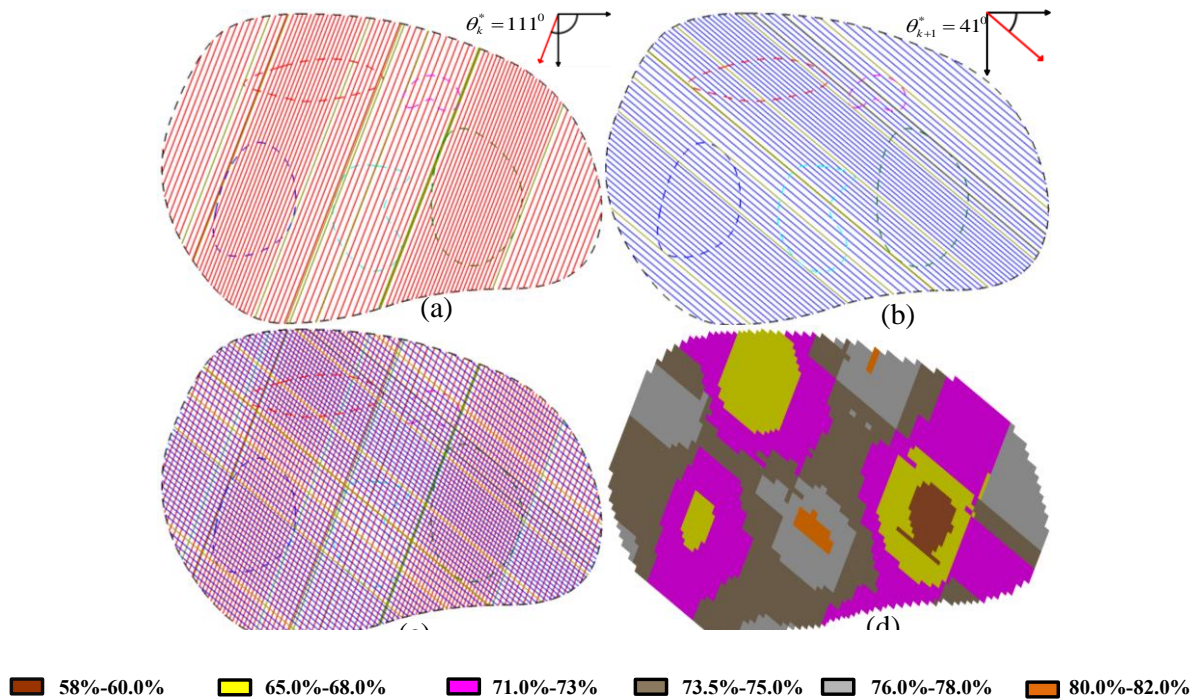


Figure 11: Variational filament locations following the porosity function (a) for the 1st layer (b) consecutive 2nd layer (c) combined layer (d) porosity gradient for the combined layer (designed with 100 micrometer filament diameter).

55.5%-57.0% 72.0%-73.0% 75.0%-77% 53.5%-55.0% 61.0%-63.0% 63.0%-64.0%

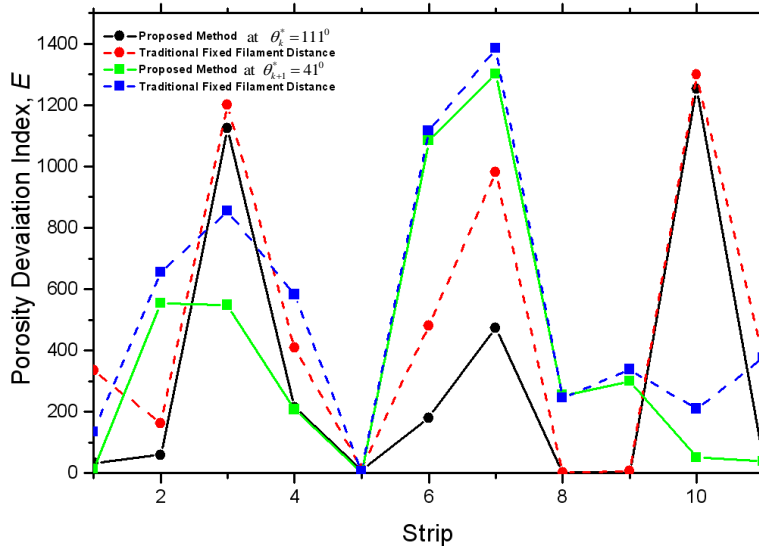


Figure 12: Porosity deviation index for both layer compared with proposed method and average 65% porosity.

The deviation data has also been calculated using Equation 5 and compared and plotted with average 65% homogeneous porosity in the Figure 12. The plot shows a significant reduction in deviation compare to the traditional equidistant filament deposition.

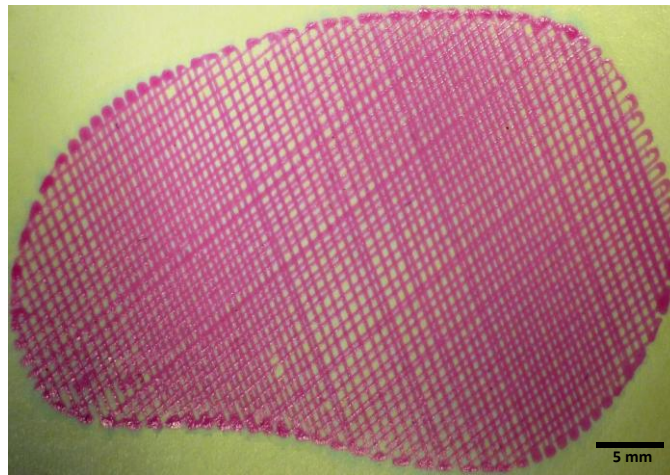


Figure 13: Sample fabrication of the model with 250 micro meter filament diameter.

A sample designed layer has been bio-fabricated using a micro-nozzle biomaterial deposition system [13] shown in Figure 13. For demonstration purpose, two consecutive slices with a uniform distance of 250 micron apart have been fabricated. The fabricated structure clearly shows the spatial variation of pore following the internal heterogeneity of the architecture.

4. Conclusion

In this research, a novel scaffold modeling approach for heterogeneous porosity has been developed. The design methodology generates spatial variational porosity following the heterogeneity of the internal regions. Attaining the exact porosity with a controllable, continuous and fabricatable design is highly unlikely, but the proposed method minimizes the deviation between the desired and design property. Moreover the proposed techniques provide better control over the porosity in heterogeneous space along with the structural continuity and fabricatability.

References

- [1] Sobral, J. M., Caridade, S. G., Sousa, R. A., Mano, J. F., and Reis, R. L., 2011, "Three-dimensional plotted scaffolds with controlled pore size gradients: Effect of scaffold geometry on mechanical performance and cell seeding efficiency," *Acta Biomaterialia*, 7(3), pp. 1009-1018.
- [2] Khoda, A. K. M. B., Ozbolat, I. T., and Koc, B., 2011, "Engineered Tissue Scaffolds With Variational Porous Architecture," *Journal of Biomechanical Engineering*, 133(1), p. 011001.
- [3] Khoda, A. B., and Koc, B., 2011, "Designing Functional Porosity in Heterogeneous Bone Tissue Scaffolds with Variational Filament Modeling," *CAD* (Submitted).
- [4] Geffre, C. P., Margolis, D. S., Ruth, J. T., DeYoung, D. W., Tellis, B. C., and Szivek, J. A., 2009, "A novel biomimetic polymer scaffold design enhances bone ingrowth," *Journal of Biomedical Materials Research Part A*, 91A(3), pp. 795-805.
- [5] Rho, J.-Y., Kuhn-Spearing, L., and Zioupos, P., 1998, "Mechanical properties and the hierarchical structure of bone," *Medical Engineering & Physics*, 20(2), pp. 92-102.
- [6] Novitskaya, E., Chen, P.-Y., Lee, S., Castro-Cesefia, A., Hirata, G., Lubarda, V. A., and McKittrick, J., 2011, "Anisotropy in the compressive mechanical properties of bovine cortical bone and the mineral and protein constituents," *Acta Biomaterialia*, 7(8), pp. 3170-3177.
- [7] Zioupos, P., Cook, R. B., and Hutchinson, J. R., 2008, "Some basic relationships between density values in cancellous and cortical bone," *Journal of Biomechanics*, 41(9), pp. 1961-1968.
- [8] Verhulp, E., van Rietbergen, B., and Huiskes, R., 2008, "Load distribution in the healthy and osteoporotic human proximal femur during a fall to the side," *Bone*, 42(1), pp. 30-35.
- [9] Dalstra, M., and Huiskes, R., 1995, "Load transfer across the pelvic bone," *Journal of Biomechanics*, 28(6), pp. 715-724.
- [10] Keaveny, T. M., Morgan, E. F., Niebur, G. L., and Yeh, O. C., 2001, "Biomechanics of trabecular bone," *Annual Review of Biomedical Engineering*, 3, pp. 307-333
- [11] Lin, J. C., Amling, M., Newitt, D. C., Selby, K., Srivastav, S. K., Delling, G., Genant, H. K., and Majumdar, S., 1998, "Heterogeneity of Trabecular Bone Structure in the Calcaneus Using Magnetic Resonance Imaging," *Osteoporosis International*, 8(1), pp. 16-24.
- [12] Wagermaier, W., Gupta, H. S., Gourrier, A., Paris, O., Roschger, P., Burghammer, M., Riekel, C., and Fratzl, P., 2007, "Scanning texture analysis of lamellar bone using microbeam synchrotron X-ray radiation," *Journal of Applied Crystallography*, 40(1), pp. 115-120.
- [13] Khoda, A., Ozbolat, I. T., and Koc, B., 2011, "A functionally gradient variational porosity architecture for hollowed scaffolds fabrication," *Biofabrication*, 3(3), pp. 1-15.